Chapter 10

Long Term Voltage Control

Mohammed Ahsan Adib Murad*, Massimiliano Chiandone†, Giorgio Sulligoi†, and Federico Milano*

**School of Electrical & Electronic Engineering, University College Dublin, †Department of Engineering and Architecture, University of Trieste*

ABSTRACT

This chapter discusses voltage controllers in distribution systems and their interactions with Converter-Interfaced Generation (CIG). The focus of the chapter is on the long-term dynamic response of the system with particular emphasis on voltage stability analysis. Two scenarios are considered: (i) Under-Load Tap Changer (ULTC) transformers coupled with distribution networks that include wind generation; and (ii) a Secondary Voltage Regulation (SVR) that coordinates solar photo-voltaic power plants. Different models and implementations of the ULTC logic as well as of the SVR are considered and discussed in detail. The first scenario is concerned on the impact of CIG on the operation of ULTCs, while the second scenario discusses how CIG can effectively contribute to the voltage regulation of the network.

KEYWORDS

Voltage Control, Converter-Interfaced Generation (CIG), Under-load Tap Changer (ULTC), Stochastic processes, Secondary Voltage Control (SVC)

10.1 INTRODUCTION

Long-term voltage control is aimed at maintaining the voltage magnitude of buses at the transmission and distribution levels within a given range and properly share the reactive power among available resources. Traditionally, long-term controllers are the voltage control of Under-Load Tap Changers (ULTCs) transformers that interface transmission and distribution networks and, in some countries, the Secondary Voltage Regulation (SVR) that coordinates the reactive power supply of conventional synchronous machines. This chapter discusses these two controllers but with an unconventional focus. In fact, the interaction of ULTCs with and the coordination of a SVR of Renewable Energy Sources (RESs) is presented and illustrated through several examples.

10.1.1 ULTC Transformers

Most transformers in distribution networks and, in particular, those interfacing the transmission with the distribution systems, have under-load tap changing

capability. The modeling of such transformers is crucial for voltage stability analysis [1] due to the presence of non-linearity (dead band, time delay, discrete tap positions) in these transformers. Even though the circuit model of tap changing transformers is well known, the model of the controller of such devices differs depending on the applications and/or implementations [2].

As the integration of stochastic distributed renewable energy resources increases, undesirable voltage fluctuations are observed in different levels of power systems. While this behavior is expected, to properly reproduce the precise dynamic behavior of ULTC regulators through simulations is not a trivial task. Moreover, as thoroughly discussed in this chapter, the implementation of the ULTC controller significantly impacts on the overall system dynamic response. This chapter addresses this modeling issue from a dynamic point of view, considering stochastic variation of the load power consumption and wind power generation at the distribution system level.

The effect of stochastic distributed generation such as wind power and photovoltaic on the frequency of tap change and performance of the ULTCs have been studied in [3, 4, 5]. These studies are relevant from the economic point of view as 50% of maintenance cost of such transformers is related to the number of tap operations. However, the aforementioned studies are based on step-wise power flow solutions, and do not consider the dynamic behavior of ULTC controllers. Studies based on time domain or quasi-steady-state simulations are considered in [6] and [7], respectively. These references do not consider stochastic modeling.

Most of the previous studies showed the behavior of ULTC transformers considering either steady-state power flow or quasi steady-state analyses. This is adequate enough for the appraisal of power system operation. However, when considering a short period, e.g. within a time frame of 5 to 15 minutes, stochastic fluctuations due to loads and distributed generation can lead to variations of the tap changers that might not be captured using a steady-state or quasi-steady state approaches. That is why the focus of this chapter is on ULTC operations occurring in a time scale of 15 minutes.

10.1.2 Secondary Voltage Regulation

Similarly to the Automatic Generation Control (AGC), the SVR is a regional control that coordinates several (conventional) generation units and allows uniformly sharing the reactive power generation among such units. Unlikely the AGC, however, the SVR is not particularly common among TSOs. While SVR is implemented manually by some TSOs, e.g. PJM and MISO in US [8], RTE in France and ENEL in Italy were pioneers in the design and implementation of automatic SVR schemes. Recently, SVR has been adopted in other countries, e.g. South Africa [9].

The SVR allows reducing the risk of shortage of reactive power in the system and thus of the occurrence of Limit-Induced Bifurcations (LIBs). In an ideal scenario, in fact, the generators that participate to the SVR reach their reactive

power limit at the same time, thus leading to a multiple LIB rather than to a sequence of LIBs. This, in general, allows a higher loading level of the system. It has been argued, for example, that if the SVR had actually been in place and properly working, the blackout that shut down the whole Italian peninsula in 2003 would not have happened [10].

The increasing penetration of CIG has led to the need to utilize such devices to support the regulation of the network. The first obvious regulators to be implemented were primary controllers of voltage and frequency. With regard to voltage support, it is now commonly accepted that RES power plants should not work at constant unitary power factor, regardless the fact that they are connected to the transmission network or to the distribution network. Moreover, as noticed in [11], existing SVR based on reactive power sources offered by traditional fossil fuels power plants shows limited controlling capability when new RES generators replace equivalent amounts of power from traditional thermal and hydro-electric large plants.

For these reasons and thanks to the development of efficient communication systems, SVR has also been considered for applications to distributed generation including wind and solar PV power plants, e.g. [12, 13, 14] and microgrids, e.g. [15, 16]. It thus appears feasible and sensible, to implement secondary controllers also for CIG, whose installed capacity has considerably increased worldwide in recent years [17].

Several proposals on the utilization of Solar Photo-Voltaic Generation (SPVG) for voltage support are available. For example, in [18], the authors propose to modulate the reactive power for voltage control functionality and bound the active power injected ramp where as, in [19], the authors propose to operate PV power plants as STATCOM devices. In this vein, recent regulation by the Italian Grid Code impose for all PV plants to be able to follow a voltage reference signal remotely send by the TSO and to modulate the reactive power exchanged by the plant according to a signal from the TSO.

Since power plants based on RES, and specifically SPVG, are more often than not connected to LV and MV distribution networks, several countries have issued specific connection rules. For example, in Italy, [20] and [21] concern connection rules of PV power plants to LV and MV, respectively. The standards above specify that a PV plant has to be equipped with proper control systems in order to provide:

- Control of the active power injected;
- Control of the reactive power injected or absorbed;
- Low voltage ride-through functionality; and
- Remote disconnection functionality.

A considerable number of plants are connected directly to the HV national transmission grid. Only in Italy 170 PV plants have a nominal power greater than 5 MW and a few dozen are connected with the HV grid (at least all of these with a power greater than 10 MW). For these power plants connected to the HV grid,

other than the TSO grid code, usually other regulations have been published. In [22] a general exposition of rules to be applied in all Europe can be found. The possibility to use the connected PV units in the provision of the reactive power compensation ancillary service is shown in [23], which discusses the well-known dynamic reactive power compensation obtained through appropriate control scheme of power electronics devices [24].

10.1.3 Organization

The remainder of this chapter is organized as follows. Section 10.2 presents the discrete and continuous models of ULTCs and their controllers for dynamic studies and discusses the dynamic response of such devices considering both deterministic and stochastic scenarios. The latter includes load and wind speed models formulated as stochastic differential equations which properly capture the probability distribution and autocorrelation of the stochastic processes. Section 10.3 presents a SVR scheme for large PV power plants with one HV connection point of a hierarchical control strategy similar to that in use in high voltage transmission networks. This control unit basically implements the Reactive Power Regulators (RPRs) of the SVR that is discussed in the Italian Grid Code.

10.2 UNDER-LOAD TAP CHANGER

Transformers are ubiquitous in transmission and distribution systems. They connect sections of the network at different voltage levels. Depending on the system structure, these transformers are:

- Step-up transformers at generator terminals;
- Transformers connecting different transmission voltage levels; and
- Transformers feeding a distribution system.

Voltage control through changing transformer ratios by using “taps” at different voltage level is a common strategy. For example transformers feeding to a distribution system compensate changes in the voltage due to changes in the load without interruption employing a automatic tap changing mechanism. Such transformers are often known as Load Tap Changing (LTC) or Under-Load Tap Changer (ULTC) or On Load Tap Changing (OLTC) transformer. Details of fundamentals on transformers can be found in [25]. We describe next the modeling of the circuit of ULTC transformers as well as a variety of discrete and continuous voltage control schemes.

10.2.1 Modeling

The general scheme of an ULTC transformer with automatic voltage control is shown in Figure 10.1. Three main physical components compose such transformers: (i) an automatic voltage regulator; (ii) a tap changer with a switching

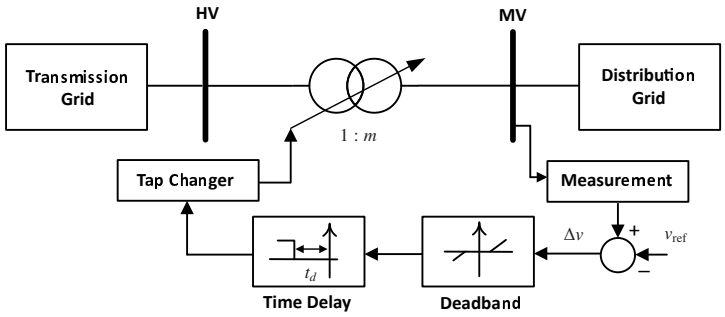

FIGURE 10.1 A tap-changer under-load transformer with a voltage controller.

mechanism; and (iii) the main transformer.

The voltage regulator includes: (i) a measuring element to measure the voltage (or reactive power) on the connected bus; (ii) a unit to compare the difference between measured and reference quantity; (iii) a dead band element that reduces the sensitivity of the controller; and (iv) a time-delay element that limits the number of variations of the tap position.

The tap changer selects a tap to change from the previous position using a switching principal and there exists several switching mechanism. Few commonly found mechanisms are: the high speed resistor type, the reactor type and the vacuum type [26]. The whole process of the tap changer is achieved through a driving mechanism.

An illustration of the switching sequence of a resistor-oil type ULTC comprising a diverter switch and a tap selector in Figure 10.2. The tap selector first selects the tap at no load (see (a)-(c) in Figure 10.2). Next, the diverter switch transfers the load current selected tap from the tap in operation (see (d)-(g) in Figure 10.2). A driving mechanism completes the switching tasks.

10.2.1.1 ULTC Circuit

Figure 10.3 shows the equivalent circuit of a two-winding transformer assuming the tap is on the primary [27]. As $\bar{v}'_h = \bar{v}_h/m$, the currents injections at buses h' and k are:

$$\begin{bmatrix} \bar{i}'_h \\ \bar{i}_k \end{bmatrix} = \bar{y}_T \begin{bmatrix} \frac{1}{m^2} & -\frac{1}{m} \\ -\frac{1}{m} & 1 \end{bmatrix} \begin{bmatrix} \bar{v}_h \\ \bar{v}_k \end{bmatrix}, \tag{10.1}$$

where bold face indicates complex numbers. Considering the physical buses h and k and including magnetization and iron losses on the primary winding (see Figure 10.4), one obtains:

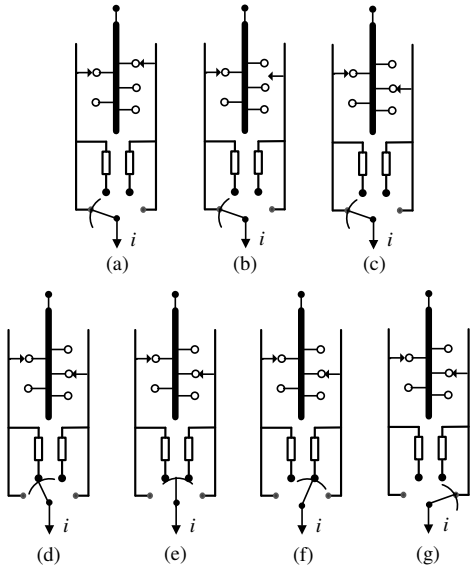

FIGURE 10.2 Sequence of switching of tap changer: tap selector (a-c) and diverter switch (d-g) [26].

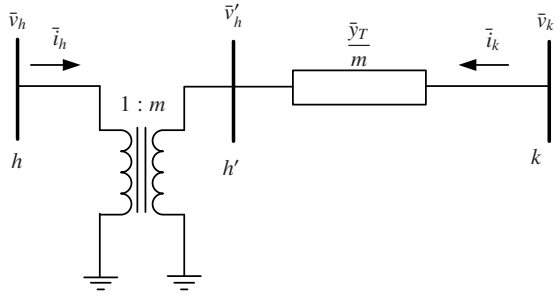

FIGURE 10.3 Equivalent circuit of the transformer with tap ratio module and series impedance.

$$\begin{bmatrix} \bar{i}_h \\ \bar{i}_k \end{bmatrix} = \begin{bmatrix} g_{\text{Fe}} + jb_\mu + \bar{y}_T \frac{1}{m^2} & -\bar{y}_T \frac{1}{m} \\ -\bar{y}_T \frac{1}{m} & \bar{y}_T \end{bmatrix} \begin{bmatrix} \bar{v}_h \\ \bar{v}_k \end{bmatrix}, \tag{10.2}$$

where $\bar{y}_T = (r_T + jx_T)^{-1}$; g_{Fe}, b_μ, r_T and x_T are transformer iron loss, magnetizing susceptance, resistance and reactance respectively. Finally, the power

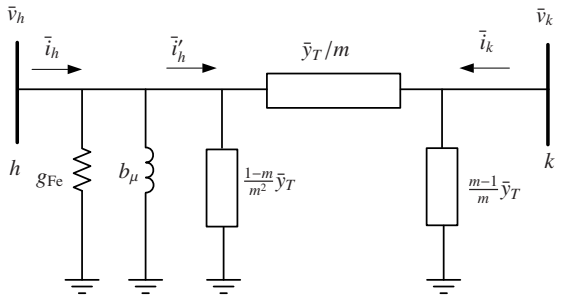

FIGURE 10.4 Equivalent circuit of a transformer.

injections at buses h and k are:

$$\begin{aligned} p_h &= v_h^2(g_{\text{Fe}} + g_T/m^2) - v_h v_k(g_T \cos\theta_{hk} + b_T \sin\theta_{hk})/m \\ q_h &= -v_h^2(b_\mu + b_T/m^2) - v_h v_k(g_T \sin\theta_{hk} - b_T \cos\theta_{hk})/m \\ p_k &= v_k^2 g_T - v_h v_k(g_T \cos\theta_{hk} - b_T \sin\theta_{hk})/m \\ q_k &= -v_k^2 b_T + v_h v_k(g_T \sin\theta_{hk} + b_T \cos\theta_{hk})/m \ . \end{aligned} \tag{10.3}$$

10.2.1.2 ULTC Control

In principle, all the elements that compose the ULTC voltage controller should be properly modeled. In the literature, however, mostly only simplified models are considered [1]. In this section, two commonly used control models are considered based on the references [1, 2, 28, 29], namely, (i) the discrete model and (ii) the continuous model.

10.2.1.2.1 Discrete model

In this model, the tap ratio m is a discrete variable that can take only fixed values in the range of $m^{\max}$ and $m^{\min}$ by a fixed step Δm. The tap ratio can move up or down by one step Δm if the controlled voltage v_k deviates more than a given dead band db with respect to the reference voltage v^{ref} for longer than a given period Δt. The switching logic of the tap ratio is:

$$m(t) = m(t - \Delta t) + f\big(e(t), c(t), \tau(t)\big)\ \Delta m \ , \tag{10.4}$$

where e models the dead band, f the time delay, c is a memory function that stores the time elapsed since the tap change and $\tau = \tau_d + \tau_m$ is the time delay. τ_d is the adjustable time delay of the controller and τ_m mechanical switching time

delay. The e and c are expressed as:

$$e(\Delta v(t), m(t-\Delta t), db, m^{\max}, m^{\min}) = \begin{cases} 1, & \text{if } \Delta v(t) > db \text{ and } m(t-\Delta t) < m^{\max} \\ -1, & \text{if } \Delta v(t) < -db \text{ and } m(t-\Delta t) > m^{\min} \\ 0, & \text{otherwise ,} \end{cases} \tag{10.5}$$

$$c(e(t), c(t-\Delta t)) = \begin{cases} c(t-\Delta t) + \Delta t, & \text{if } e(t) = 1 \text{ and } c(t-\Delta t) \geq 0 \\ c(t-\Delta t) - \Delta t, & \text{if } e(t) = -1 \text{ and } c(t-\Delta t) \leq 0 \\ 0, & \text{otherwise ,} \end{cases} \tag{10.6}$$

$$\tag{10.7}$$

where t is the current simulation time, $t - \Delta t$ is the previous simulation step.

The function f depends upon the mode of operation: sequential or non-sequential mode. The timer is reset after each tap change in non-sequential mode whereas in sequential mode the timer is reset only after the voltage is back within the dead band range. The function f is as follows:

- For non-sequential mode,

$$f\big(e(t), c(t), \tau(t)\big) = \begin{cases} 1, & \text{if } e(t) = 1 \text{ and } c(t) > \tau(t) \\ -1, & \text{if } e(t) = -1 \text{ and } c(t) < \tau(t) \\ 0, & \text{otherwise ,} \end{cases} \tag{10.8}$$

- For sequential mode,

$$f\big(e(t), c(t), \tau(t)\big) = \begin{cases} 1, & \text{if } e(t) = 1 \text{ and } c(t) > \tau(t) \text{ ,} \\ & \text{for subsequent taps if } e(t) = 1 \text{ and } c(t) > \tau_m(t) \\ -1, & \text{if } e(t) = -1 \text{ and } c(t) > \tau(t) \text{ ,} \\ & \text{for subsequent taps if } e(t) = -1 \text{ and } c(t) > \tau_m(t) \\ 0, & \text{otherwise ,} \end{cases} \tag{10.9}$$

The time delay τ can be fixed or variable. In case of variable time delay, the higher the voltage error the faster the tap change. Depending on different time-delay settings four different discrete models are considered for both sequential and non-sequential mode and summarized below:

- D1: both delays are fixed, $\tau_d = \tau_{d,0}$ and $\tau_m = \tau_{m,0}$;
- D2: τ_d is combination of fixed and variable time, $\tau_d = \tau_{d,0} \cdot \frac{db}{|\Delta v|} + \tau_{d,1}$ and τ_m is fixed, $\tau_m = \tau_{m,0}$;
- D3: τ_d is variable, $\tau_d = \tau_{d,0} \cdot \frac{db}{|\Delta v|}$ and τ_m is fixed, $\tau_m = \tau_{m,0}$;
- D4: both delays are variable, $\tau_d = \tau_{d,0} \cdot \frac{db}{|\Delta v|}$ and $\tau_m = \tau_{m,0} \cdot \frac{db}{|\Delta v|}$.

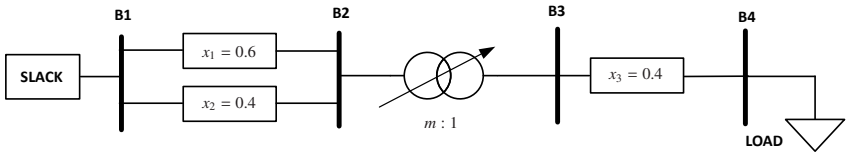

FIGURE 10.5 A single generator connected to an infinite bus [30].

TABLE 10.1 Base case parameters of the test system of Figure 10.5

Component	*Parameters*
Discrete Model	$db = 4\%$, $\Delta m = 0.0125$, $\tau_{d,0} = 15$, $\tau_{d,1} = 5$, $\tau_{m,0} = 8$
Continuous Model	$H = 0.001$, $K = 0.043$
All ULTCs	$m^{\max} = 1.1$, $m^{\min} = 0.8$, $r_t = 0$, $x_t = 0.4$
Load	$p_o = 0.4$ pu(MW), $T_p = 5$ s, $\alpha_t = 2$, $\alpha_s = 0$

10.2.1.2.2 Continuous model

The continuous control model approximates the tap ratio step Δm to be small, so that tap ratio m can vary continuously. The time delays are approximated as a lag transfer function and the tap ratio differential equation is given by:

$$\dot{m}(t) = -Hm(t) + K\left(v_k(t) - v_{\text{ref}}\right), \quad m^{\min} \leq m(t) \leq m^{\max} \tag{10.10}$$

where H, K, v_k and v_{ref} are the integral deviation, inverse time constant, secondary bus voltage and controlled reference voltage, respectively. The dead band is not included in this model. Note that it is possible to create an equivalent continuous model of each discrete model [2].

10.2.2 Examples

The impact of the voltage control action of different ULTC controller implementations to the long-term voltage stability is studied in this section using deterministic case studies.

10.2.2.1 Case Study 1

The test system consists of four buses, one slack bus, one tap changing transformer, three transmission lines and one dynamic load. The scheme of this test system, which is based on [30], is shown in Figure 10.5. Data are given in Table 10.1.

The continuous dynamics of the real power load in bus 4 considered as a first order dynamic exponential recovery load given by:

$$\begin{aligned} T_p \dot{x}_p(t) &= -x_p(t) + p_o(v_t(t)^{\alpha_s} - v_t(t)^{\alpha_t}) \\ p_L(t) &= x_p(t) + p_o v_t(t)^{\alpha_t}, \end{aligned} \tag{10.11}$$

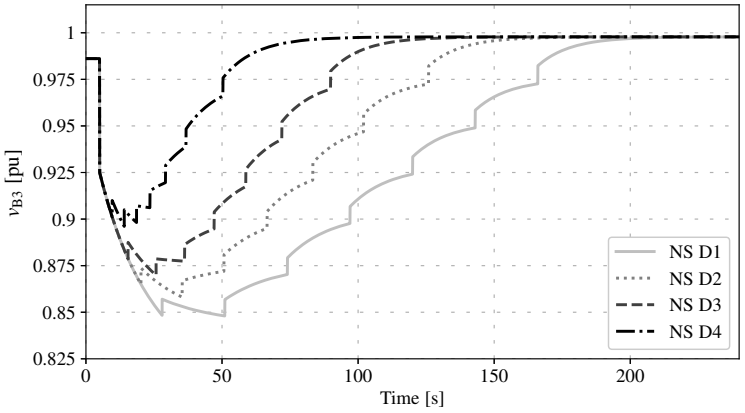

FIGURE 10.6 Voltage magnitude at bus 3 using non-sequential discrete ULTC models.

where, x_p is the load state driving the actual load demand p_L, v_t is the voltage at the load bus and p_o is the nominal active power load. The load undergoes an initial transient given by the term $p_o v_t^{\alpha_t}$ during a voltage disturbance and recovery of the load dictated by the time constant T_p.

The contingency consists of a line outage ($x = 0.4$) between B1 and B2 at $t = 5$ s. Figures 10.6-10.7 show the trajectories of voltage at bus 3 for non-sequential and sequential discrete models respectively.

Following the disturbance, the voltage response is faster using the sequential models compared to the non-sequential models. This is due to the reset logic of the time delay. Comparing all non-sequential models (NS D1 - NS D4) and sequential models (S D1 - S D4), the voltage response is comparatively faster when moving from delay settings D1 to D4 because the time delay changes dynamically depending on the voltage deviation. Moreover, all ULTCs restore the voltage at the same voltage so number of tap operation is same for all ULTCs. These results indicate that the sequential model with variable time delay (D4) restores the voltage within the dead band compared to all other discrete tap changers.

10.2.2.2 Case Study 2

The Nordic test system presented in [31] is used for the second deterministic case study. The system includes 74 buses; 102 branches, of which 20 step-up and 22 distribution transformers with ULTCs; 20 generators, of which 7 are round rotor and 13 are salient pole types, with Turbine Governors (TGs), Automatic Voltage Regulations (AVRs), Power System Stabilizers (PSSs), and Over-Excitation Limiters (OELs). All models used in this case study match those reported in [31], except for the OELs, which are modeled as in [27]. The parameters of all devices are also given in [31]. All distribution transformers

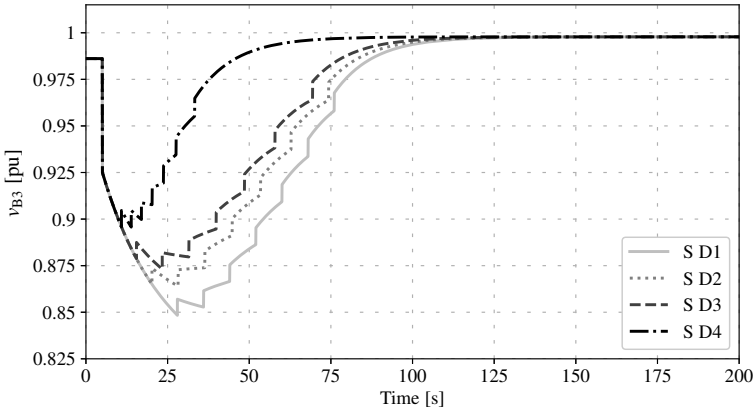

FIGURE 10.7 Voltage magnitude at bus 3 using sequential discrete ULTC models.

TABLE 10.2 Delays of ULTCs

Transformer	Delays			Transformer	Delays		
	τ_{d0}	τ_{d1}	τ_m		τ_{d0}	τ_{d1}	τ_m
11-1011	30	5	8	41-4041	31	5	9
12-1012	30	5	9	42-4042	31	5	10
13-1013	30	5	10	43-4043	31	5	11
22-1022	30	5	11	46-4046	31	5	12
1-1041	29	5	12	47-4047	30	5	8
2-1042	29	5	8	51-4051	30	5	9
3-1043	29	5	9	61-4061	30	5	10
4-1044	29	5	10	62-4062	30	5	11
5-1045	29	5	11	63-4063	30	5	12
31-2031	29	5	12	71-4071	31	5	9
32-2032	31	5	8	72-4072	31	5	11

are equipped with a ULTC controller with dead band $db = 2\%$, maximum and minimum tap position are $m^{\max} = 1.2$ and $m^{\min} = 0.8$ with step size $\Delta m = 0.01$. The values for the time delays are given in Table 10.2.

The system consists of four areas: North, Central, Equivalent and South. The base case of the system is heavily loaded with large power transfers from North to Central areas.

The comparison discussed in this section considers the dynamic response following a three-phase fault at bus 4032, occurring at $t = 1$ s and cleared at $t = 1.06$ s by opening the line between buses 4032-4044. Transient response of voltage of a distribution bus at the Central area is shown Figures 10.8-10.9 for non-sequential and sequential discrete tap changers respectively.

The line trip following the fault forces power to flow North-Central corridor over the remaining lines. However, the reactive power capabilities of the Central

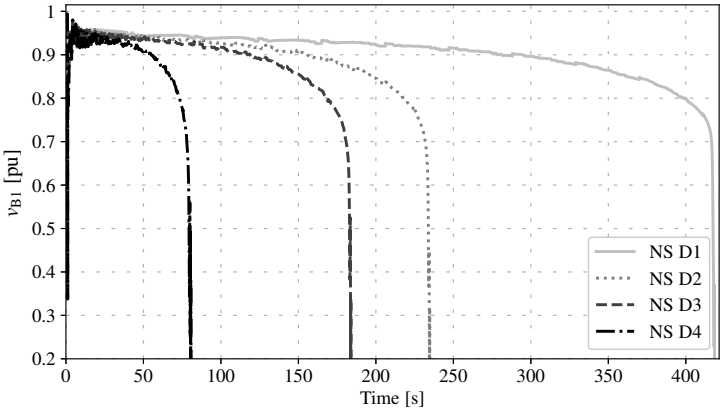

FIGURE 10.8 Voltage magnitude at bus 1 using non-sequential discrete ULTC models.

and Northern generators impacts the maximum power delivered to the Central loads. On the other hand, the ULTCs try to restore the voltages of the distribution buses and load powers. In this case, however, the amount of power that the ULTCs have to restore is greater than the maximum power that can be delivered by the generation and the transmission system and, hence, a voltage instability occurs, which eventually leads to a voltage collapse. The collapse occurs in the time scale of minutes, hence the notation *long-term voltage instability*.

Similar to Case Study 1 in Section 10.2.2.1, due to the dependency of the time delay of the tap switching on the voltage error, non-sequential and sequential ULTC controllers show different transient responses. Of course, due to its slow response, the non-sequential ULTCs controllers take a longer time than sequential ULTC controllers to drive the system to collapse.

10.2.3 Stochastic Modeling

This section outlines the load consumption and wind speed models considered in the stochastic case study discussed in the example of Section 10.2.4. These models include stochastic perturbations modeled by means of the following Itô-type differential equation:

$$\dot{\eta}(t) = a\big(\eta(t), t\big) + b\big(\eta(t), t\big)\, \xi(t)\ , \tag{10.12}$$

where η is the state variable that describes the stochastic process, a and b are the drift and the diffusion terms respectively, and ξ is the white noise, i.e. the formal time derivative of the Wiener process [32]. Equation (10.12) is a general expression that can take into account both Gaussian and non-Gaussian processes and is thus appropriate to model load power variations [33] and wind speed fluctuations [34].

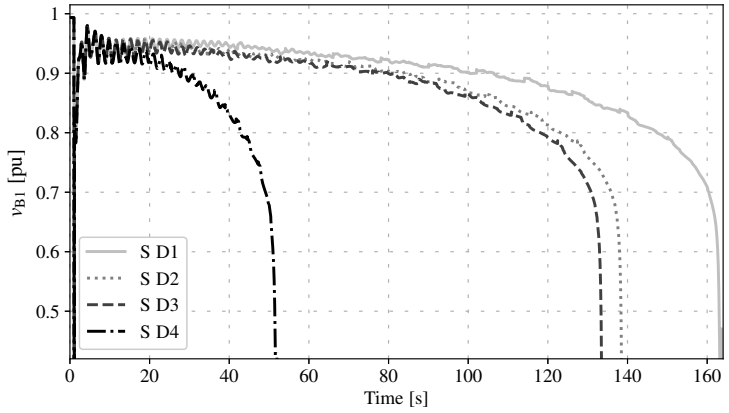

FIGURE 10.9 Voltage magnitude at bus 1 using sequential discrete ULTC models.

10.2.3.1 Voltage Dependent Load

The well-known Voltage Dependent Load (VDL) model is given by [27]:

$$\begin{aligned} p_L(t) &= -p_{L,o}(v(t)/v_o)^\gamma \\ q_L(t) &= -q_{L,o}(v(t)/v_o)^\gamma, \end{aligned} \tag{10.13}$$

where $p_{L,o}$ and $q_{L,o}$ are the active and reactive powers at the the nominal voltage v_o; v is the voltage magnitude of the bus where the load is connected; and γ is the power exponent.

Merging together the stochastic equation (10.12) and the load equations (10.13) lead to a Stochastic VDL (SVDL) load model. Since load variations are approximately Gaussian and show a constant standard deviation, we define the diffusion terms a and b in (10.12) to resemble an Ornstein-Uhlenbeck process [33]. The resulting SVDL load model is:

$$\begin{aligned} p_L(t) &= (-p_{L,o} + \eta_p(t))(v(t)/v_o)^\gamma \\ q_L(t) &= (-q_{L,o} + \eta_q(t))(v(t)/v_o)^\gamma \\ \dot{\eta}_p(t) &= \alpha_p(\mu_p - \eta_p(t)) + b_p\xi_p(t) \\ \dot{\eta}_q(t) &= \alpha_q(\mu_q - \eta_q(t)) + b_q\xi_q(t), \end{aligned} \tag{10.14}$$

where the α terms are the speed at which the stochastic variables η are "attracted" towards the mean values μ, and the b terms represents the volatility of the processes.

10.2.3.2 Wind Speed

To emulate the wind speed, a and b in (10.12) must be defined so that the probability distribution of η is a Weibull process. It is also important to reproduce

the autocorrelation of the wind speed, which is assumed to be exponentially decaying. This can be achieved through the regression theorem and the stationary Fokker-Planck equation, as thoroughly discussed in [34]. The resulting drift and diffusion terms are:

$$\begin{aligned} a\big(\eta(t)\big) &= -\alpha \cdot \big(\eta(t) - \mu_{\mathrm{W}}\big) \\ b\big(\eta(t)\big) &= \sqrt{b_1\big(\eta(t)\big) \cdot b_2\big(\eta(t)\big)}\,, \end{aligned} \tag{10.15}$$

where α is the autocorrelation coefficient; μ_{W} is the mean of the Weibull distribution; and

$$\begin{aligned} b_1\big(\eta(t)\big) &= \frac{2\,\alpha}{p_{\mathrm{W}}\big(\eta(t)\big)} \\ b_2\big(\eta(t)\big) &= \lambda \cdot \Gamma\left(1 + \frac{1}{k}, \left(\frac{\eta(t)}{\lambda}\right)^{k}\right) - \mu_{\mathrm{W}} \cdot e^{-(\eta(t)/\lambda)^{k}}\,, \end{aligned}$$

where p_W is the Weibull Probability Density Function (PDF); Γ is the incomplete Gamma function; k and λ are the shape and scale parameters of the Weibull distribution, respectively.

10.2.4 Example

The test network considered in this example is a small Irish distribution system with both radial and meshed configurations [35, 36]. The network includes eight buses, six loads, two wind generation, one slack bus and eight transmission lines. The operating nominal voltage of B1-B8 is 38 kV and the buses are fed by an ULTC type step down transformer from a 110 kV network. The network topology is shown in Figure 10.10. Network parameters can be found in [35].

The active and reactive power loading of the system are 15.02 MW and 8.29 MVAr respectively and the nominal wind farm capacities are 12 MW and 20 MW at B5 and B3 respectively. 5% of the loads is a SVDL modeled as in (10.14) and the 95% is modeled as constant PQ ($\gamma = 0$ in (10.14)). The wind generator model is a 5th-order doubly-fed induction generator with variable-speed wind turbine having discrete pitch control, first-order AVR, turbine governor and Maximum Power Point Tracking (MPPT). The input to wind turbine is a stochastic wind modeled as in (10.15).

Five different case studies are considered for different delay and dead band settings of the discrete ULTC models. 500 15-minute Monte Carlo simulations are considered for each model and parameter set. The average number of tap operations using sequential type ULTCs for different dead band and time delay settings are given in Table 10.3. As expected, the higher the time delay and dead band, the lower the number of tap changes. This case study only considers sequential type ULTCs. Due to the stochastic variation of the load and wind speed, non-sequential ULTC controller models also yield similar results as sequential types because of similar delay logic of first tap switch.

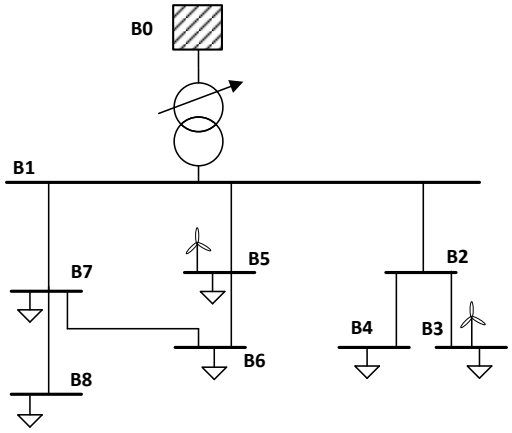

FIGURE 10.10 Topology of the test distribution network [35, 36].

TABLE 10.3 Average number of tap operations using sequential discrete models

Cases	Parameter			D1	D2	D3	D4
	db	τ_{d0}	τ_{m0}				
C1	2.2	15	8	4.40	3.46	4.72	7.94
C2	2.4	15	8	2.43	2.23	2.56	2.60
C3	2.5	15	8	1.79	1.68	1.83	1.85
C4	2.5	20	10	1.60	1.43	1.64	1.66
C5	3	15	8	0.97	0.95	0.97	0.97

Figures 10.11 and 10.12 show 500 trajectories of the voltage at bus 1 for cases C1 and C5 (see Table 10.3) with D1 type discrete model. These figures also include the mean, μ, and $\mu \pm 3\sigma$, where σ is the standard deviation. The mean and the standard deviation of the 500 trajectories are calculated at every time instant of the simulation interval which is 0.01 s. The average voltage trajectory is similar in both figures, however C1 shows more than four times the tap operations of C5. Thus stochastic variations are important to take account for preventing unnecessary tap changes.

10.2.5 Remarks

The deterministic and stochastic case studies discussed above show that dead band and delay settings of ULTCs play crucial role for the voltage restoration or collapse and number of tap operation. When considering stochastic processes, the time domain analysis is necessary to properly account for ULTC tap variations as these cannot be rightly captured considering steady-state analysis. Simulation results also allow concluding that, depending on the ULTC control model, the number of tap operation can be significantly different, so it is important to accurately implement the right control logic. This is another aspect that cannot

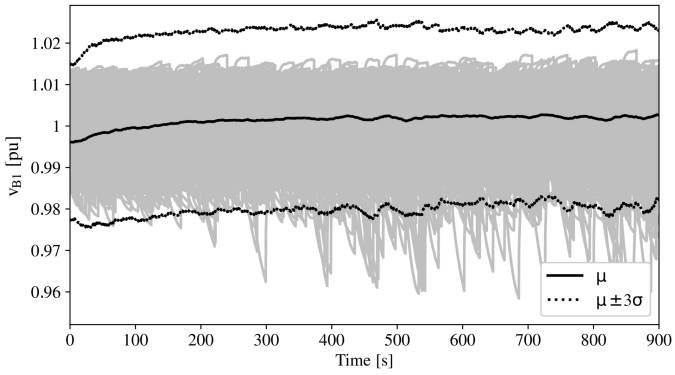

FIGURE 10.11 500 stochastic trajectories and statistical properties of the bus 1 voltage using sequential discrete model (D1) for case C1.

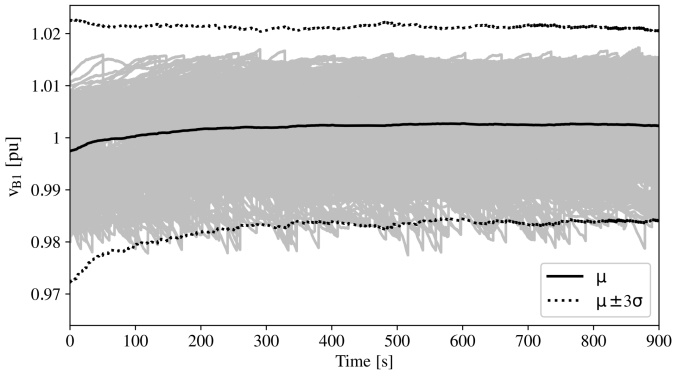

FIGURE 10.12 500 stochastic trajectories and statistical properties of the bus 1 voltage using sequential discrete model (D1) for case C5.

be captured by conventional steady-state analyses.

10.3 SECONDARY VOLTAGE REGULATION

This section focuses on voltage regulation for large PV power plants and proposes the application to large PV power plants of a hierarchical control strategy similar to that in use in HV transmission networks [37]. A central control unit coordinates the reactive power of each converter to regulate the voltage of the point of connection. Commercially available converters usually accept as references the following signals: reactive power, power factor or grid voltage. This control unit basically implements the Reactive Power Regulators (RPRs) of the Secondary Voltage Regulation (SVR) that is discussed in the Italian Grid Code. The interested reader can find a comprehensive description of the Italian SVR

scheme in [38].

While we discuss only applications to PV power plants, the hierarchical voltage control scheme discussed in this section can be applied to different kinds of power plants connected to HV networks. For example, references [39] and [40] show that such a control can be successfully used for cluster of hydro power plants and wind farms, respectively, participating to TSO voltage regulation.

The application of a unique control system, for both traditional power plants and RES, allows standardizing the system dynamic response and increases the overall stability of the network.

10.3.1 Control Strategy

Figure 10.13 shows a synoptic scheme of the SVR. It is assumed that, at the point of connection, the PV has to provide the voltage control capability as discussed in [11]. The SVR controller receives the reference voltage from the TSO. The pilot bus is the point of connection of the PV power plant. Then, an external voltage control loop, implemented by the Busbar Voltage Regulator (BVR), computes a reference of reactive power level q_{lev} ($q_{\text{lev}} \in [-1, 1]$), which is then multiplied by the vector of the capability of each generator.

The resulting vector q_{ref} of reactive power limits is then compared with the actual reactive power of each generator. The error is then processed by the Dynamic Decoupling (DD) block and sent to the Generator Reactive Power Regulators (GRPRs) [42]. The DD block is key for the dynamic response of the system and is further discussed in the following section. The resulting GRPRs output control signals are used as reference signals for the conventional voltage control of the converter. It is also possible to exclude the external voltage control loop and send a q_{lev} reference signal directly to the reactive power control loop.

Several studies exist on the possibility to control reactive power of a VSC independently from the active power. In [43] the transient response of the reactive power to the change of reactive power reference is shown. The results show also the decoupling of the p and q injections. The fast response for the reactive power control can be found also in [44]. Therefore, in the remainder of this chapter, the converters are simplified with a first order model.

The control system shown in Figure 10.13 presents specific features, such as speed of response and accuracy of the steady-state response. Moreover, it ensures the stability of the system, even in case of asymmetrical disturbances (thanks to the dynamic decoupling array), and the ability to allocate quotas of reactive power among the different generators according to the actual needs and contingencies. The control system shown in Figure 10.13 is also simple to implement (as it is based only on one common signal q_{ref}) and is well-known by the national TSO as it has been applied to conventional power plants that participate to the secondary voltage control.

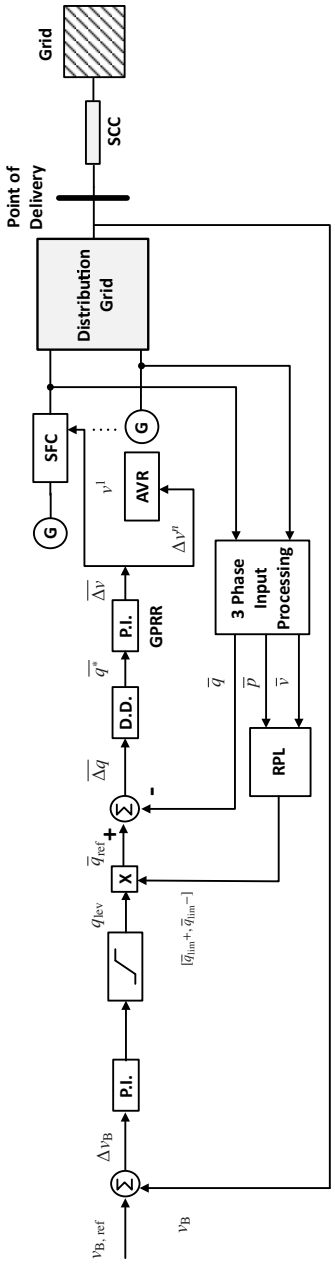

FIGURE 10.13 Synoptic scheme of the secondary voltage regulation [41].

10.3.2 Coupling of Large RES Power Plants

Large RES power plants that are connected to the HV transmission system are typically composed of a set of generators connected through a MV distribution network and having a single Point of Connection (PoC) at HV level. For the sake of example, Figure 10.17 shows the topology of a real-world cluster of hydro-electric power plant. The MV distribution network can be described by the well-known power flow equations, as follows:

$$\begin{aligned} p_k &= \sum_{i=1}^{n} v_k v_i Y_{ki} \cos\left(\theta_k - \theta_i - \gamma_{ki}\right) - p_{o,k},\ k = 1, 2, \ldots, n\ , \\ q_k &= \sum_{i=1}^{n} v_k v_i Y_{ki} \sin\left(\theta_k - \theta_i - \gamma_{ki}\right) - q_{o,k},\ k = 1, 2, \ldots, n\ , \end{aligned} \tag{10.16}$$

where p, q, v, Y, θ and γ are the generator active power at node, the generator reactive power at node, the node voltage, the module of admittance coefficients, the phase angle of the node voltage and the phase angle of the admittance coefficients respectively. Finally p_o and q_o are the active and reactive load power consumptions, respectively, at the network buses. Linearizing (10.16) at a given operating point leads to the following matrix form:

$$\begin{bmatrix} \Delta \boldsymbol{p} \\ \Delta \boldsymbol{q} \end{bmatrix} = \begin{bmatrix} \boldsymbol{p_v} & \boldsymbol{p_\theta} \\ \boldsymbol{q_v} & \boldsymbol{q_\theta} \end{bmatrix} \times \begin{bmatrix} \Delta \boldsymbol{v} \\ \Delta \boldsymbol{\theta} \end{bmatrix} \tag{10.17}$$

where $\Delta \boldsymbol{p}$, $\Delta \boldsymbol{q}$, $\Delta \boldsymbol{v}$ and $\Delta \boldsymbol{\theta}$ are the vectors of the power and voltage variations; and the Jacobian matrices $\boldsymbol{p_v} = \frac{\partial \boldsymbol{p}}{\partial \boldsymbol{v}}$, $\boldsymbol{p_\theta} = \frac{\partial \boldsymbol{p}}{\partial \boldsymbol{\theta}}$, $\boldsymbol{q_v} = \frac{\partial \boldsymbol{q}}{\partial \boldsymbol{v}}$, and $\boldsymbol{q_\theta} = \frac{\partial \boldsymbol{q}}{\partial \boldsymbol{\theta}}$ represent the link between the active and reactive power with the module and bus voltage phasors. The elements of the Jacobian matrices embed the information on the characteristic parameters of the transmission lines of the network. For the purposes of the voltage control, active power variations are neglected, hence leading to:

$$\Delta \boldsymbol{q} = \boldsymbol{q_v}\, \Delta \boldsymbol{v}\ , \tag{10.18}$$

from where it appears that $\boldsymbol{q_v}$ defines the electric coupling between generator reactive powers and voltage magnitudes. We assume that $\boldsymbol{q_v}$ is full rank, as it is in most practical applications. The discussion of idiosyncratic cases where $\boldsymbol{q_v}$ is singular is out of the scope of this chapter.

Starting from the inverse of the electric coupling matrix it is possible to calculate the dynamic decoupling matrix, as follows:

$$\mathbf{D} = \boldsymbol{q_v}^{-1}\ , \tag{10.19}$$

where $\mathbf{D}$ is formally defined as $\frac{\partial \boldsymbol{v}}{\partial \boldsymbol{q}}$ and is thus defined as:

$$\Delta \boldsymbol{v} = \mathbf{D}\, \Delta \boldsymbol{q}\ . \tag{10.20}$$

Note that the coefficients of matrix $\mathbf{D}$ can also be calculated through a numerical sensitivity analysis, as discussed in [42].

10.3.3 Examples

10.3.3.1 Case Study 1

The proposed SVR scheme is applied to a real PV plant of a nominal power of 48 MVA connected to the high voltage transmission grid. Each photovoltaic field (made of series and parallel connected photovoltaic modules) is connected to two centralized, i.e. equipped with a unique MPPT, converters. The low voltage converter outputs are raised to 20 kV via a double winding transformer in 45 "converter stations." The output of each converter station is connected with the output of the nearby station forming four groups which are connected to a central station from where four medium voltage circuits are sent to a transforming station. In the transforming station, the four circuits are connected to the medium voltage side of a transformer that raises the voltage up to 132 kV that is the nominal voltage of the transmission line where the PV plant is connected. The single line diagram of the plant topology is shown in [41].

Simulations have been carried out assuming an initial $v_{B,\text{ref}} = 1.005$ pu and same reactive power injections from all generators. At $t = 500$ s, the reference voltage $v_{B,\text{ref}}$ step to 1.03 pu; consequently, the regulator imposes a new value of reactive power to be supplied by the generators. Figure 10.14 shows the voltage profile at the point of delivery as wel as the trajectory of the reactive power delivered by the generator expressed in pu with respect to its nominal power.

As expected, the proposed control allows distributing the reactive power equally among the generators of the power plant; furthermore there is no steady-state error, the dynamic of the system does not show oscillations. The dynamic response of the proposed control scheme is thus very similar to that of a SVR installed in conventional power plants.

10.3.3.2 Case Study 2

Three network topologies are considered. These are depicted in Figures 10.15-10.17. Based on the method described in the previous paragraph, it is also possible to calculate the sensitivity coefficients $\mathbf{D}$ that combine the PoC N0 to all other nodes of the grid.

Table 10.4 shows, for all the three example plants, the influence of each generator on the voltage variations at the point of delivery. If all values have similar magnitude, the generators can effectively and similarly participate to the voltage regulation.

For all network topologies, regulator coefficients and time constants are chosen to ensure stability and a dynamic similar to those of traditional power plants. The internal voltage loop, e.g. AVR, is characterized by fast timescale in the order of tenths of a second; the RPR has a time constant of few seconds and finally the external voltage loop (BVR) time constant is typically of the order of 10 s.

The first simulation has been solved considering topology A. Two generators connected to a common bus bar are working in asymmetrical states (the reactive

power of the generators are different although their nominal power is equal). At time $t = 50$ s the SVR is switched on trying to equate the reactive power of both generators. Without the decoupling matrix (see Figure 10.18), reactive power oscillations occur (all reactive power plots are in per unit of 100 MVA). The oscillations are in phase quadrature which implies a reactive power flow between the generators.

Although the topology of the network A and its initial operating conditions has been chosen to emphasize the coupling phenomenon, such asymmetric perturbations happens every time the system is started or a single generator is inserted into the cluster. Figure 10.19 shows the effect of the same perturbation on the system when the decoupling matrix is included in the SVR. In this case, transients are exponentially decaying and do not oscillate. This kind of reactive

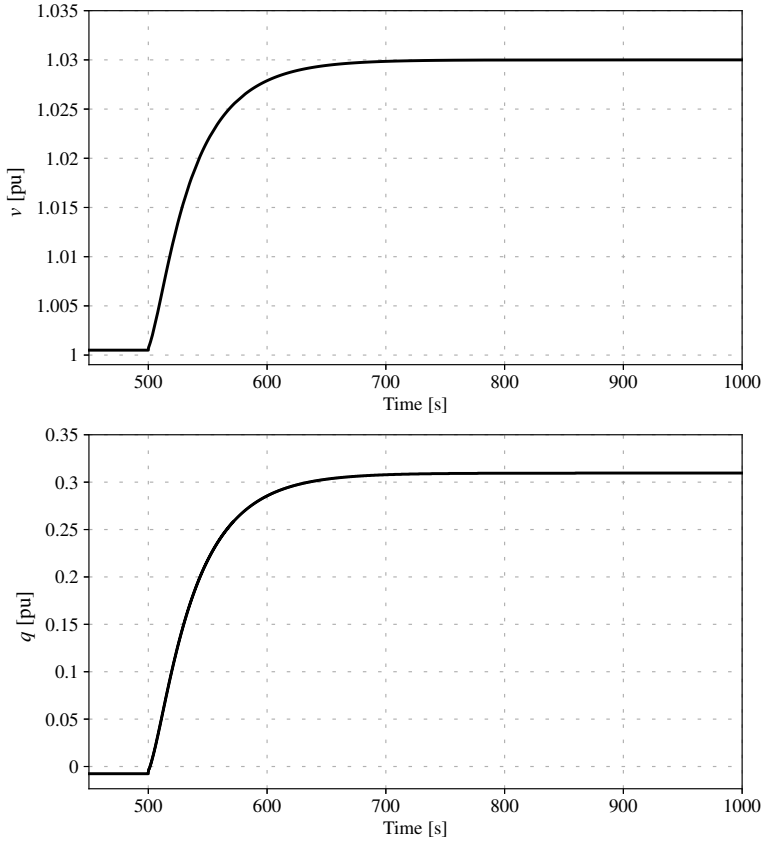

FIGURE 10.14 Case study 1: Voltage profile at the point of connection and generator reactive power [41].

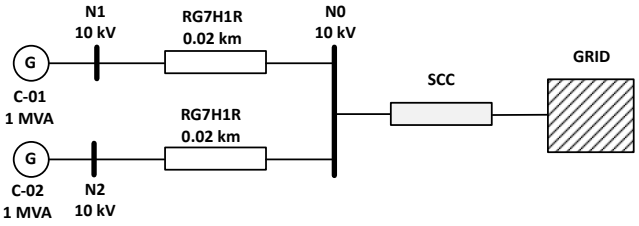

FIGURE 10.15 Topology of plant A [45].

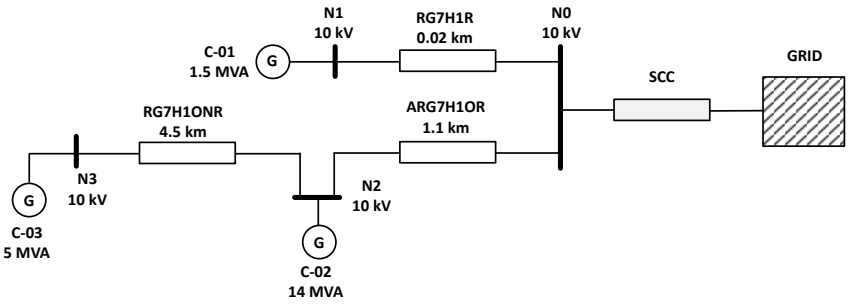

FIGURE 10.16 Topology of plant B [45].

power flow among generators has to be limited for several reasons: it represents a stress conditions for alternators, causes additional losses, can interfere with voltage protections, represents a voltage disturbance for load directly fed by the generators.

Figures 10.20 and 10.21 show the step response of the voltage reference for the network topology B respectively without and with the DD matrix. Figures 10.22 and 10.23 show similar results for the topology C. In particular, reactive power responses in Figures 8 and 10 demonstrate the positive effect of the decoupling action: no flow of reactive power occurs among generators. It is worth noticing that this phenomenon is not appreciable looking only at the voltage response.

TABLE 10.4 Sensitivity coefficients [45]

$\frac{\partial v}{\partial q}$	N0	Plant	$\frac{\partial v}{\partial q}$	N0	Plant
G1	0.777	Plant A	C-02	0.0714	Plant C
G2	0.777		C-03	0.0675	
G1	0.634	Plant B	C-04.GR1	0.0680	
G2	0.610		C-04.GR2	0.0680	
G3	0.593		C-05	0.0689	
C-01	0.0717	Plant C	C-06	0.0657	

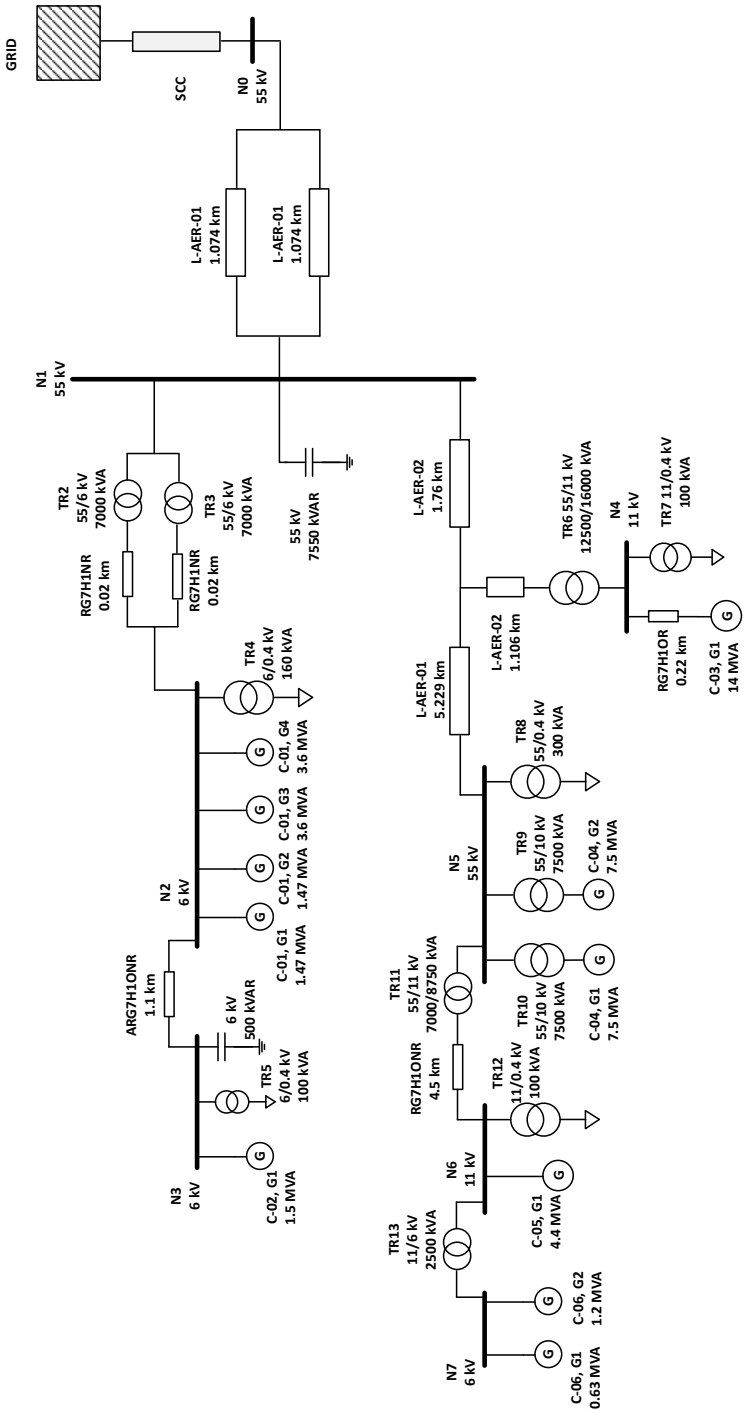

FIGURE 10.17 Topology of plant C [45].

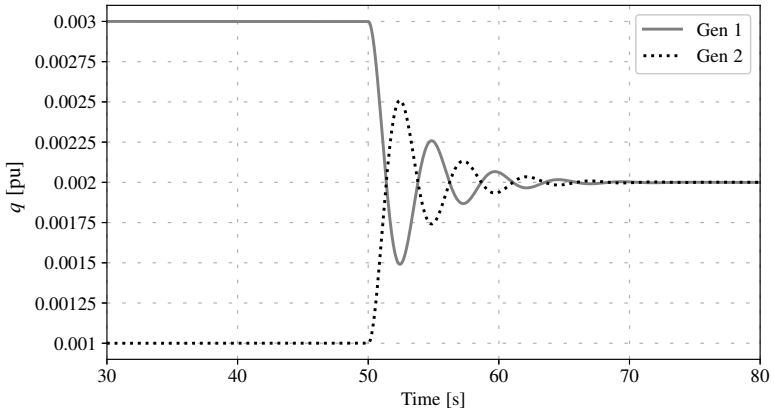

FIGURE 10.18 Network A: Reactive power response without dynamic decoupling [45].

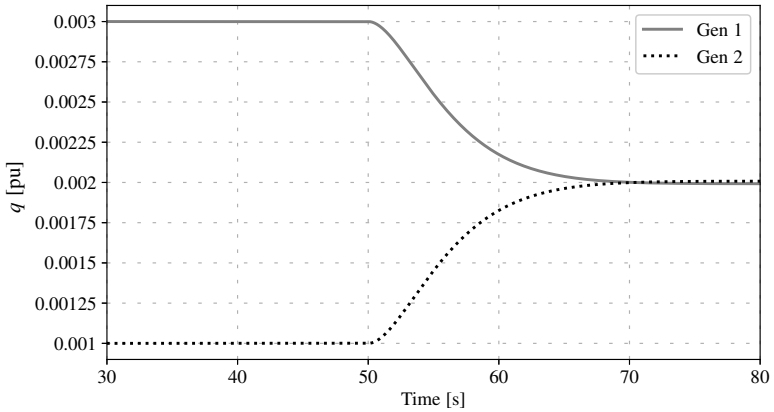

FIGURE 10.19 Network A: Reactive power response with dynamic decoupling [45].

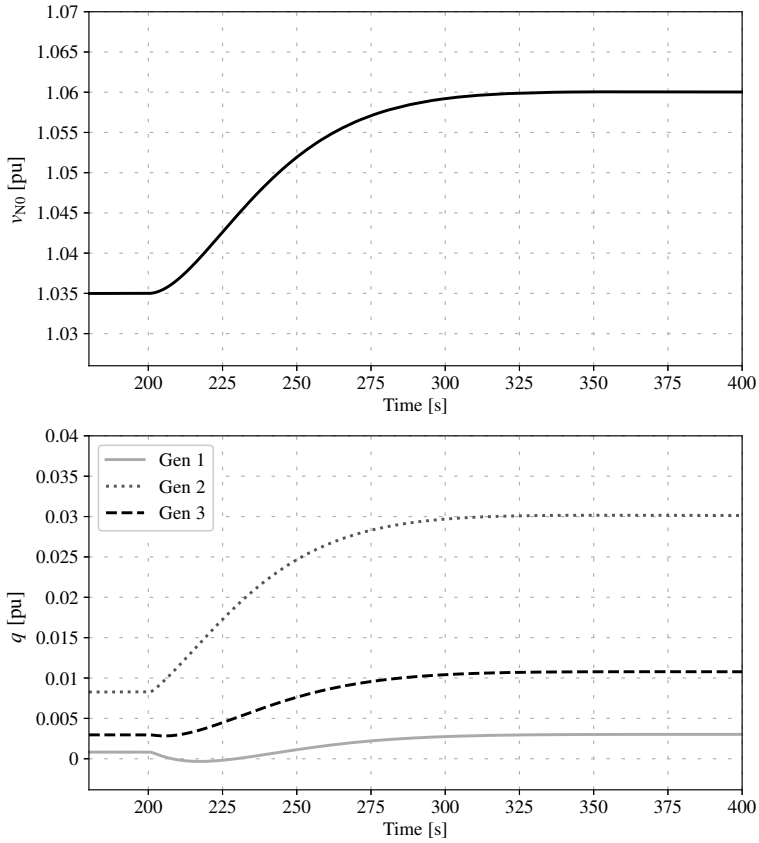

FIGURE 10.20 Network B: Voltage and reactive power response for a step in reference voltage without the decoupling matrix [45].

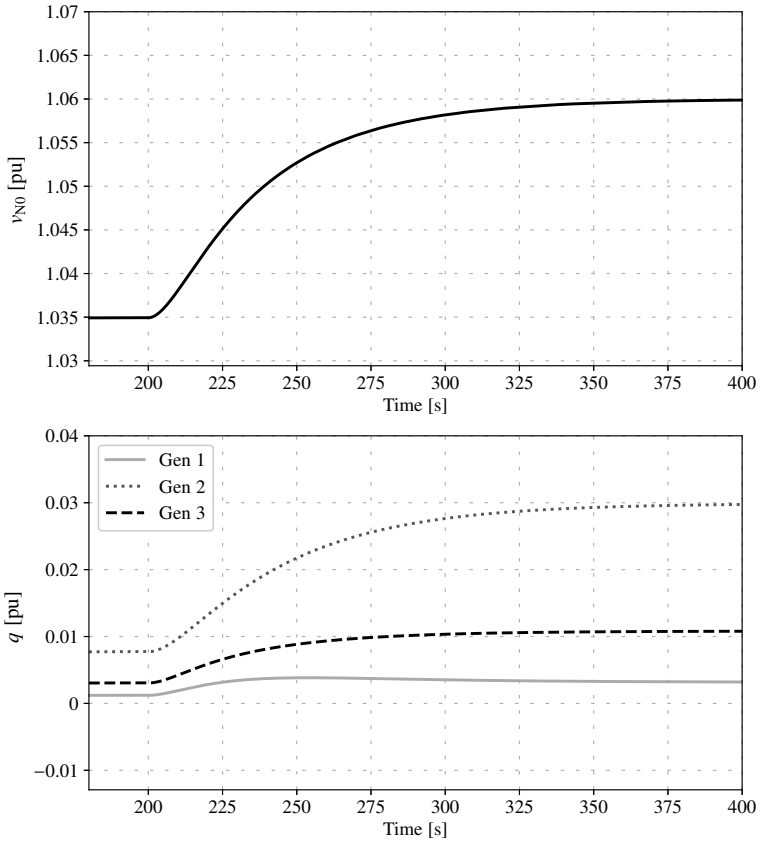

FIGURE 10.21 Network B: Voltage and reactive power response for a step in reference voltage with the decoupling matrix [45].

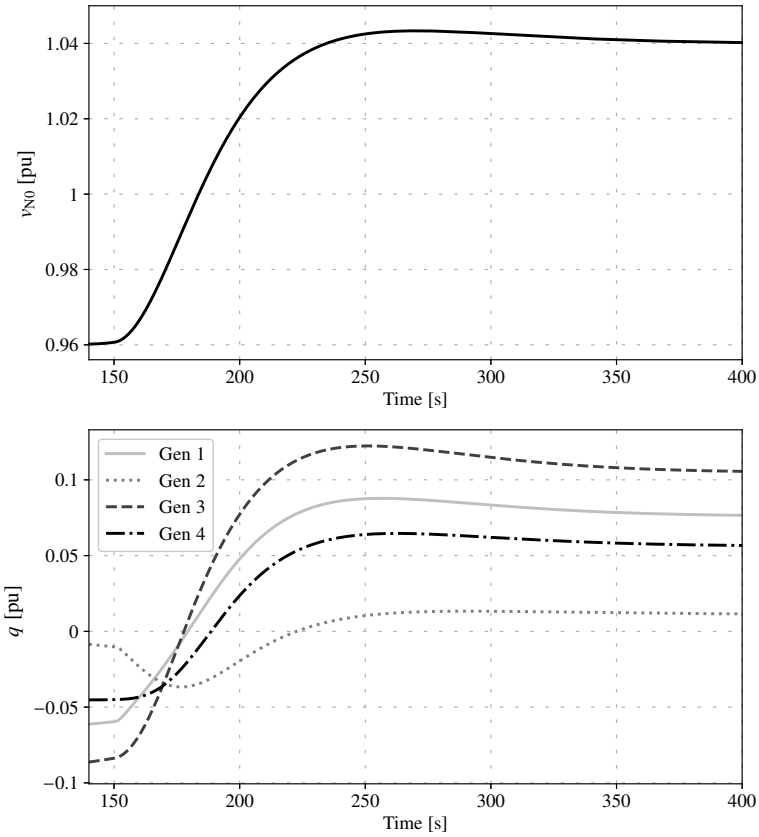

FIGURE 10.22 Network C: Voltage and generators reactive power response without decoupling matrix [45].

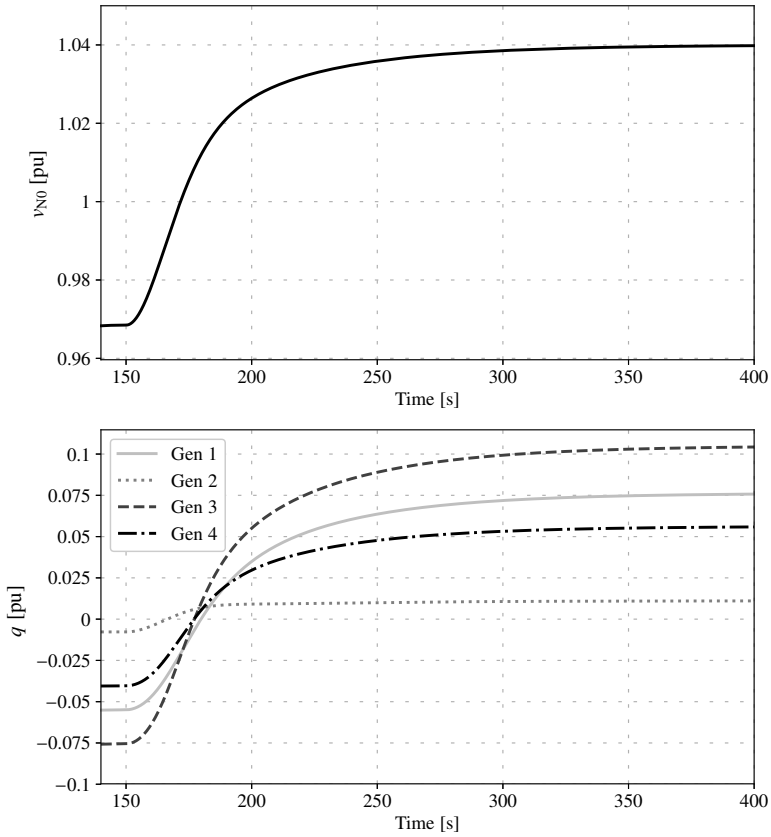

FIGURE 10.23 Network C: Voltage and generators reactive power response with decoupling matrix [45].

BIBLIOGRAPHY

[1] T. Van Cutsem and C. Vournas, *Voltage stability of electric power systems*. Springer Science & Business Media, 2007.

[2] F. Milano, "Hybrid control model of under load tap changers," *IEEE Transactions on Power Delivery*, vol. 26, no. 4, pp. 2837–2844, 2011.

[3] S. N. Salih, P. Chen, and O. Carlson, "The effect of wind power integration on the frequency of tap changes of a substation transformer," *IEEE Transactions on Power Systems*, vol. 28, no. 4, pp. 4320–4327, Nov 2013.

[4] S. S. Baghsorkhi and I. A. Hiskens, "Impact of wind power variability on sub-transmission networks," in *IEEE PES General Meeting*, July 2012, pp. 1–7.

[5] C. Long, A. T. Procopiou, L. F. Ochoa, G. Bryson, and D. Randles, "Performance of OLTC-based control strategies for LV networks with photovoltaics," in *IEEE PES General Meeting*, July 2015, pp. 1–5.

[6] D. Ranamuka, A. P. Agalgaonkar, and K. M. Muttaqi, "Examining the interactions between DG units and voltage regulating devices for effective voltage control in distribution systems," *IEEE Transactions on Industry Applications*, vol. 53, no. 2, pp. 1485–1496, March 2017.

[7] G. K. Ari and Y. Baghzouz, "Impact of high PV penetration on voltage regulation in electrical distribution systems," in *International Conference on Clean Electrical Power (ICCEP)*, June 2011, pp. 744–748.

[8] Y. Song and M. Begović, "Secondary voltage and stability control," in *15th International Power Electronics and Motion Control Conference (EPE/PEMC)*, September 2012, pp. LS2b.4–1–LS2b.4–7.

[9] S. Corsi, F. De Villiers, and R. Vajeth, "Power system stability increase by secondary voltage regulation applied to the south africa transmission grid," in *IREP Symposium Bulk Power System Dynamics and Control - VIII (IREP)*, August 2010, pp. 1–18.

[10] S. Corsi and C. Sabelli, "General blackout in Italy Sunday September 28, 2003, h. 03:28:00," in *IEEE PES General Meeting*, June 2004, pp. 1691–1702.

[11] M. Chiandone, G. Sulligoi, S. Massucco, and F. Silvestro, "Hierarchical voltage regulation of transmission systems with renewable power plants: An overview of the Italian case," in *Renewable Power Generation Conference (RPG)*, Sep. 2014, pp. 1–5.

[12] L. Yu, D. Czarkowski, and F. de Leon, "Optimal distributed voltage regulation for secondary networks with DGs," *IEEE Transactions on Smart Grid*, vol. 3, no. 2, pp. 959–967, June 2012.

[13] M. E. Moursi, G. Joos, and C. Abbey, "A secondary voltage control strategy for transmission level interconnection of wind generation," *IEEE Transactions on Power Electronics*, vol. 23, no. 3, pp. 1178–1190, May 2008.

[14] W. Xiao, K. Torchyan, M. S. El Moursi, and J. L. Kirtley, "Online supervisory voltage control for grid interface of utility-level PV plants," *IEEE Transactions on Sustainable Energy*, vol. 5, no. 3, pp. 843–853, July 2014.

[15] S. Peyghami, H. Mokhtari, P. Davari, P. C. Loh, and F. Blaabjerg, "On secondary control approaches for voltage regulation in DC microgrids," *IEEE Transactions on Industry Applications*, vol. 53, no. 5, pp. 4855–4862, Sep. 2017.

[16] Y. Xu, H. Sun, W. Gu, Y. Xu, and Z. Li, "Optimal distributed control for secondary frequency and voltage regulation in an islanded microgrid," *IEEE Transactions on Industrial Informatics*, vol. 15, no. 1, pp. 225–235, Jan 2019.

[17] J. von Appen, M. Braun, T. Stetz, K. Diwold, and D. Geibel, "Time in the sun: The challenge of high PV penetration in the german electric grid," *IEEE Power & Energy Magazine*, vol. 11, no. 2, pp. 55–64, March 2013.

[18] J. Arrinda, J. A. Barrena, M. A. Rodriguez, and A. Guerrero, "Analysis of massive integration of renewable power plants under new regulatory frameworks," in *International Conference on Renewable Energy Research and Application (ICRERA)*, Oct 2014, pp. 462–467.

[19] R. K. Varma and M. Salama, "Large-scale photovoltaic solar power integration in transmission and distribution networks," in *IEEE PES General Meeting*, July 2011, pp. 1–4.

[20] "Norma italiana CEI 0-16," Tech. Rep., December, 2012.

[21] "Norma italiana CEI 0-21," Tech. Rep., December, 2012.

[22] AISBL and ENTSOE, "Entso-e network code for requirements for grid connection applicable to all generators," *ENTSO-E AISBL: Brussels, Belgium*, 2012.

[23] F. Delfino, R. Procopio, M. Rossi, and G. Ronda, "Integration of large-size photovoltaic systems into the distribution grids: a P-Q chart approach to assess reactive support capability," *IET Renewable Power Generation*, vol. 4, no. 4, pp. 329–340, July 2010.

[24] H. K. Tyll and F. Schettle, "Historical overview on dynamic reactive power compensation solutions from the begin of AC power transmission towards present applications," in *IEEE PES Power Systems Conference and Exposition*, March 2009, pp. 1–7.

[25] A. C. Franklin and D. P. Franklin, *The J & P transformer book: a practical technology of the power transformer*. Elsevier, 2016.

[26] D. Dohnal, "On-load tap-changers for power transformers," Maschinenfabrik Reinhausen GmbH, Regensburg, Germany, Tech. Rep., September 2013.

[27] F. Milano, *Power system modelling and scripting*. Springer Science & Business Media, 2010.

[28] M. S. Calovic, "Modeling and analysis of under-load tap-changing transformer control systems," *IEEE Transactions on Power Apparatus and Systems*, no. 7, pp. 1909–1915, 1984.

[29] Q. Wu, D. H. Popovic, D. J. Hill, and M. Larsson, "Tap changing dynamic models for power system voltage behaviour analysis," in *Power Systems Computation Conference (PSCC)*, 1999.

[30] I. A. Hiskens and P. J. Sokolowski, "Systematic modeling and symbolically assisted

simulation of power systems," *IEEE Transactions on Power Systems*, vol. 16, no. 2, pp. 229–234, 2001.

[31] IEEE PSDP Committee Power System Stability Subcommittee Test Systems for Voltage Stability and Security Assessment Task Force, "Test systems for voltage stability analysis and security assessment," Technical Report PES-TR19, Tech. Rep., 2015.

[32] C. Gardiner, "Stochastic methods: a handbook for the natural and social sciences 4th ed.(2009)."

[33] F. Milano and R. Zárate-Miñano, "A systematic method to model power systems as stochastic differential algebraic equations," *IEEE Transactions on Power Systems*, vol. 28, no. 4, pp. 4537–4544, 2013.

[34] R. Zárate-Miñano, F. M. Mele, and F. Milano, "SDE-based wind speed models with Weibull distribution and exponential autocorrelation," in *IEEE PES General Meeting*. IEEE, 2016, pp. 1–5.

[35] C. Murphy and A. Keane, "Local and remote estimations using fitted polynomials in distribution systems," *IEEE Transactions on Power Systems*, vol. 32, no. 4, pp. 3185–3194, 2017.

[36] M. A. A. Murad, F. M. Mele, and F. Milano, "On the impact of stochastic loads and wind generation on under load tap changers," in *2018 IEEE Power Energy Society General Meeting (PESGM)*, Aug 2018, pp. 1–5.

[37] J. L. Sancha, J. L. Fernandez, A. Cortes, and J. T. Abarca, "Secondary voltage control: analysis, solutions and simulation results for the Spanish transmission system," *IEEE Transactions on Power Systems*, vol. 11, no. 2, pp. 630–638, May 1996.

[38] G. Sulligoi, M. Chiandone, and V. Arcidiacono, "Newsart automatic voltage and reactive power regulator for secondary voltage regulation: Design and application," in *2011 IEEE Power and Energy Society General Meeting*, July 2011, pp. 1–7.

[39] R. Campaner, M. Chiandone, V. Arcidiacono, G. Sulligoi, and F. Milano, "Automatic voltage control of a cluster of hydro power plants to operate as a virtual power plant," in *IEEE International Conference on Environment and Electrical Engineering (EEEIC)*, June 2015, pp. 2153–2158.

[40] M. Chiandone, R. Campaner, V. Arcidiacono, G. Sulligoi, and F. Milano, "Automatic voltage and reactive power regulator for wind farms participating to TSO voltage regulation," in *IEEE Eindhoven PowerTech*, June 2015, pp. 1–5.

[41] M. Chiandone, R. Campaner, A. M. Pavan, V. Arcidiacono, F. Milano, and G. Sulligoi, "Coordinated voltage control of multi-converter power plants operating in transmission systems. the case of photovoltaics," in *International Conference on Clean Electrical Power (ICCEP)*, June 2015, pp. 506–510.

[42] P. M. S. Carvalho, P. F. Correia, and L. A. F. M. Ferreira, "Distributed reactive power generation control for voltage rise mitigation in distribution networks," *IEEE Transactions on Power Systems*, vol. 23, no. 2, pp. 766–772, May 2008.

[43] J. C. Vasquez, R. A. Mastromauro, J. M. Guerrero, and M. Liserre, "Voltage support

provided by a droop-controlled multifunctional inverter," *IEEE Transactions on Industrial Electronics*, vol. 56, no. 11, pp. 4510–4519, Nov 2009.

[44] A. Cagnano, E. De Tuglie, M. Liserre, and R. A. Mastromauro, "Online optimal reactive power control strategy of PV inverters," *IEEE Transactions on Industrial Electronics*, vol. 58, no. 10, pp. 4549–4558, Oct 2011.

[45] R. Campaner, M. Chiandone, G. Sulligoi, and F. Milano, "Automatic voltage and reactive power control in distribution systems: Dynamic coupling analysis," in *IEEE International Conference on Renewable Energy Research and Applications (ICRERA)*, Nov 2016, pp. 934–939.